Fast Tracking of Cardiac Motion Using 3D-HARP

Li Pan*, Jerry L. Prince, *Fellow, IEEE*, João A. C. Lima, and Nael F. Osman, *Member, IEEE*

***Abstract*—Magnetic resonance (MR) tagging is capable of accurate, noninvasive quantification of regional myocardial function. Routine clinical use, however, is hindered by cumbersome and time-consuming postprocessing procedures. We propose a fast, semiautomatic method for tracking three-dimensional (3-D) cardiac motion from a temporal sequence of short- and long-axis tagged MR images. The new method, called 3-D-HARmonic Phase (3D-HARP), extends the HARP approach, previously described for two-dimensional (2-D) tag analysis, to 3-D. A 3-D material mesh model is built to represent a collection of material points inside the left ventricle (LV) wall at a reference time. Harmonic phase, a material property that is time-invariant, is used to track the motion of the mesh through a cardiac cycle. Various motion-related functional properties of the myocardium, such as circumferential strain and left ventricular twist, are computed from the tracked mesh. The correlation analysis of 3D-HARP and FINDTAGS + Tag Strain(E) Analysis (TEA), which are well-established tag analysis techniques, shows that the regression coefficients of circumferential strain (E_{CC}) and twist angle are $r^2 = 0.8605$ and $r^2 = 0.8645$, respectively. The total time required for tracking 3-D cardiac motion is approximately 10 min in a 9 timeframe tagged MRI dataset and has the potential to be much faster.**

***Index Terms*—Cardiac motion tracking, MR tagging, phase time-invariance, strain computation, 3-D-HARmonic Phase (3D-HARP).**

I. Introduction

ALTHOUGH ventricular mass, volume, and ejection fraction (EF) represent the current standard for evaluating cardiac global function, extensive research has shown that regional function measures, such as wall-thickening, strain, and torsion, may be both more specific in defining cardiac disease and more sensitive in detecting subclinical markers of LV dysfunction and myocardial diseases. For example, in patients who develop LV dilation or hypertrophy, regional function may be depressed although global function is preserved [1]. Quantification of the regional deformation of myocardial tissue is, therefore, an important objective in the characterization of LV function. In the past, physical markers were surgically implanted into the myocardium and their motion tracked using imaging. However, this method is highly invasive and the markers tend to influence the very motion that is being measured. MR tagging, proposed by Zerhouni *et al.* in 1988 [2] and Axel *et al.* in 1989 [3], provides noninvasive markers inside the myocardium which deform with the motion of the myocardium and do not affect cardiac motion. Analysis of tag motion makes it possible to quantify true regional myocardial function in a noninvasive fashion.

In general, tagged MR images are analyzed in two steps. The first step requires the identification and tracking of tags in the MR images, typically requiring a segmentation of the LV wall through identification of its outer and inner contours. The second step involves the reconstruction of three-dimensional (3-D) cardiac motion and the computation of motion-related variables, such as strain, displacement field, and torsion [4]. The first step is usually very time-consuming and relies heavily on user interaction to guarantee proper segmentation and tag tracking. For example, Guttman *et al.* [5] proposed a "template-matching" method to detect tags and an active contour method or "snake" to extract contours. Based on this approach, a software package called FINDTAGS [6] has been one of the most successful approaches for segmentation and tracking; however, it still requires several hours to complete the processing of one dataset. Denney [7], [8] used a maximum-likelihood/maximum *a posteriori* (ML/MAP) method to estimate and detect the tags without user-defined contours, and then compute LV strain. This method reduces the occurrence of false tag detections and also reduces the processing time to about 1 h.

To reconstruct 3-D cardiac motion, the second step in analyzing tagged MR images, many 3-D-model-based approaches have been developed [9], [10]. O'Dell *et al.* [11] used a displacement field fitting to reconstruct 3-D myocardial deformation. Huang, Wang, and Deng *et al.* [12]–[14] proposed different types of B-Spline model to perform spatiotemporal motion tracking. Young [15] introduced the concept of "model tags" and used a finite element model (FEM)-based method that could reconstruct 3-D heart wall motion without prior identification of ventricular boundaries and tag locations. Kerwin and Prince [16] used a deformation model to track the intersection points of tag surface or "MR markers." The performance of these methods depends entirely on the accuracy of the first step, and the methods are often computational intensive as well.

Recently, the *HARmonic Phase* (HARP) method, was developed by Osman *et al.* [17], [18]. Rather than working on the tagged images directly, HARP focuses on their Fourier transforms, where tagged patterns produce an array of energy peaks. By using a bandpass filter to isolate an off-center spectral peak in the Fourier transform of a tagged image, zero padding it and performing the inverse Fourier transform, a complex image is

Manuscript received July 30, 2004; revised January 9, 2005. This work was supported in part by the National Heart, Lung, and Blood Institute (NHLBI) under Grant HL072704 and Grant HL66075. N. F. Osman and J. L. Prince are founders of and own stock in Diagnosoft, Inc., a company that seeks to license the HARP technology. The terms of this arrangement are being managed by the Johns Hopkins University in accordance with its conflict of interest policies. *Asterisk indicates corresponding author.*

*L. Pan is with the Department of Biomedical Engineering, Johns Hopkins School of Medicine, 601 N. Caroline St. JHOC 4240, Baltimore, MD 21287 USA (e-mail: lipan@bme.jhu.edu).

J. L. Prince is with the Department of Electrical and Computer Engineering, Johns Hopkins University, Baltimore, MD 21218 USA (e-mail: prince@jhu.edu).

J. A. C. Lima is with the Department of Medicine-Cardiology, Johns Hopkins School of Medicine, Baltimore, MD 21287 USA (e-mail: jlima@jhmi.edu).

N. F. Osman is with the Department of Radiology, Johns Hopkins School of Medicine, Baltimore, MD 21287 USA (e-mail: nael@jhu.edu).

Digital Object Identifier 10.1109/TBME.2005.851490

produced. The phase of this image is called the *harmonic phase* and is directly related to the motion of the tag lines. The advantage of the HARP method is that the computation of motion from the harmonic phase is direct and rapid, with no need for prior segmentation or human interaction. However, the use of HARP to date has been in large part restricted to the tracking of two-dimensional (2-D) motion, typically on short-axis (SA) image planes. This is a serious limitation given that the heart is, of course, 3-D and has a significant component of motion in the long-axis (LA) direction. Recently, Ryf *et al.* [19] and Haber *et al.* [20] proposed 3D extensions of HARP. In [19], the HARP tracking method [17] was extended to 3-D by using a combined 3-D tagging and imaging approach. Extraction of spectral peaks in 3-D Fourier space permitted point tracking using the HARP approach throughout the volume of interest in a very natural, appealing manner. The authors of [20] pursued an approach in which a FEM was constructed within the LV wall and the HARP phase computed on a sparse collection of image planes was used to move this model throughout the cardiac cycle.

In this paper, we present a method that extends the HARP method to 3-D while maintaining the primary gains of the overall HARP approach, including both rapid processing time and minimal human interaction. Also, the phase invariance condition used in 2D-HARP tracking is extended and applied in 3-D to guarantee accurate deformation results. The method compares well to another validated technique, and provides 3-D motion quantities of practical interest in about 10 min with very little human interaction.

II. Theory

A. Basic Idea of HARP

HARP analysis concentrates on the Fourier transform of tagged MR images. Fig. 1 shows a horizontally tagged MR image [Fig. 1(a)] and its Fourier transform [Fig. 1(b)]. One dc peak at the center of Fourier space and another two harmonic spectral peaks can be seen in Fig. 1(b). A bandpass filter, shown here as a circle, is applied to isolate a spectral peak, which can be identified by the index k. The inverse Fourier transform of this isolated region produces the complex image

$$I_k(\boldsymbol{y},t) = D_k(\boldsymbol{y},t)e^{j\phi_k(\boldsymbol{y},t)} \tag{1}$$

where $\boldsymbol{y}$ is the location of a pixel on the image plane, t is the time, sampled in discrete steps and corresponding to one of the timeframes, D_k is the harmonic magnitude image, and ϕ_k is the harmonic phase (HARP) image. The harmonic magnitude image reflects the geometrical change of the heart and the image intensity change caused by fading, while the HARP image reflects the motion of the myocardium in the direction orthogonal to the tags. Technically, however, only a "wrapped" value of harmonic phase in the range of $[-\pi, +\pi)$ can be obtained, which can be shown as

$$a_k(\boldsymbol{y},t) = W\left(\phi_k(\boldsymbol{y},t)\right) \tag{2}$$

where W is a nonlinear wrapping function and a_k is the HARP angle image. The harmonic magnitude image and the HARP angle image are shown in Fig. 1 (c) and (d), respectively.

There are three main properties of the HARP image [17]. First, the locations of the wrapping transitions on the HARP angle image are closely coincident with the locations of the tag lines during myocardial motion. Second, the phase values on the HARP image are dense, providing more information than just the locations of tags lines. Finally, the HARP value is a material property of the underlying tagged tissue—i.e., the phase value of a material point is fixed from the tagging instant and does not change as long as the tags do not significantly fade. This phase invariance property is the basis of HARP tracking.

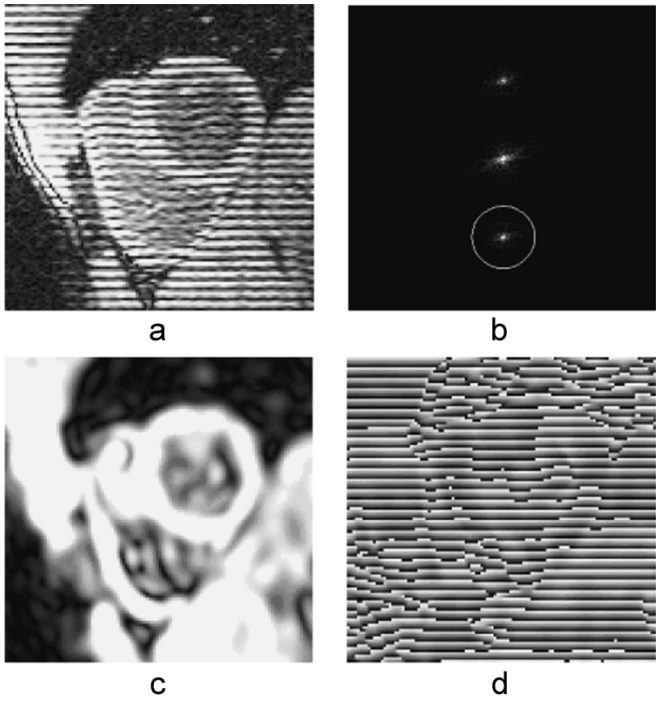

Fig. 1. (a) An MR image with horizontal tags. (b) The magnitude of the Fourier transform of the tagged MR image. The circle indicates a bandpass filter, which is applied to extract the spectral peak. (c) Harmonic magnitude image. (d) HARP angle image.

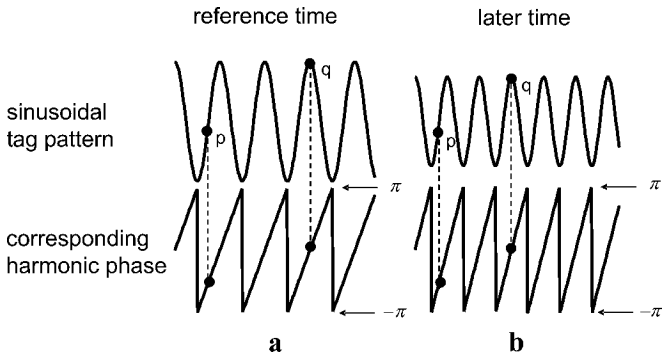

Fig. 2. The phase invariance property of material points in HARP. A sinusoidal tag pattern and its corresponding harmonic phase $[-\pi\ \pi)$ at reference time are shown in (a). At a later time, shown in (b), the tags decay in amplitude due to fading and increase in frequency because of "tissue" compression. The range of the phase in (b) is unchanged but the slope gets larger. Two material points, p and q, located on the tagged image, move with the tags and keep the same phase values at different time points.

The phase invariance property can be illustrated by a simple 1-D example in Fig. 2 [21]. Fig. 2(a) shows a sinusoidal pattern and its corresponding (wrapped) harmonic phase. Fig. 2(b) depicts the tag pattern and the phase of the same region of the tissue at a later time. Although tissue compression and tag

fading cause the tag frequency to increase and its amplitude to decrease, the corresponding harmonic phase of a material point keeps the same value at different time points—demonstrating that the HARP value is a material property of the material point. The slope of the phase is used to compute the local tissue strain and the value of the phase is used for point tracking. Due to the fact that the phase is wrapped, an assumption of small motion between two adjacent timeframes is needed to guarantee that the points can be uniquely associated.

B. Phase Invariance and Motion Tracking

HARP motion tracking uses the fact that the harmonic phase value of a material point is time-invariant. To frame this concept mathematically, consider a material point located at $\boldsymbol{x}_n \in \Re^3$ at time t_n. If $\boldsymbol{x}_{n+1}$ is the position of this point at time t_{n+1}, then the phase invariance condition states that

$$\phi(\boldsymbol{x}_{n+1}, t_{n+1}) = \phi(\boldsymbol{x}_n, t_n). \tag{3}$$

In 2D-HARP, two tag orientations, and hence, two HARP images, are sufficient to track 2-D apparent motion—i.e., the projection of 3-D motion onto a 2-D plane. Therefore, ϕ is a 2-D vector, i.e., $\phi = [\phi_1 \;\; \phi_2]^T$ in 2D-HARP. In the 3-D approach we present here, $\boldsymbol{x}_n$ and $\boldsymbol{x}_{n+1}$ are the actual 3D positions of a material point at two different times, so that ϕ is a 3-D vector, i.e., $\phi = [\phi_1 \;\; \phi_2 \;\; \phi_3]^T$, where the subscripts represent the x, y and z directions, respectively.

Although the extension to 3-D appears to be mathematically straightforward, there are a number of practical issues that make it difficult. The first issue is the requirement for three tag directions to track 3-D motion, in contrast to the two tag orientations required for 2D-HARP. A parallel "stack" of SA images with both horizontal and vertical tags and a radial array of LA images with only horizontal tags are used in this study. The combination of these tag orientations yields 3-D motion information. The images are acquired in 3 to 18 breath-holds, depending on the protocol.

This acquisition protocol, however, reveals a second issue that must be addressed. The combination of SA and LA images comprises a relative sparse 3-D coverage by tagged images. Because the images themselves are sparse, HARP phase observations are not available for every point within the heart volume. Finally, even when a point of interest does lie on an image plane (SA or LA), there is typically only one or two tag orientations providing HARP phase information at that point (the exception being for points at the intersections of SA and LA images). Therefore, both the image planes and the HARP phase information are sparse in this image acquisition protocol. This issue of sparsity has been addressed in the past by modeling the motion of the entire volume in some way. A model, whether a stochastic field fit [7] or a finite element model [15], [20], is often specified according to the underlying heart anatomy to provide connections between the sparse observations through model-based interpolation. We also impose a model to bridge information between image planes; however, our model is deliberately simple and data-driven, permitting both rapid initialization and fast tracking, which is ideally suited to the direct extension of the HARP tracking approach using phase invariance on sparse data sets.

C. The Material Mesh Model

We propose a material mesh model comprising a collection of material points inside the myocardium approximating the midwall of the LV. Let the material mesh at timeframe n be denoted by the set M_n. The mesh should be allowed to move in 3-D through the cardiac cycle in such a way that any point on the mesh, $\mu \in M_n$, maintains the same harmonic phase. We use the notation, $\psi(\mu, t)$ to denote harmonic phase as a function of material points (Lagrangian function) to distinguish it from $\phi(\boldsymbol{y}, t)$, which is harmonic phase that is a function of a spatial coordinate (Eulerian function). Using this convention, the phase invariance condition for points on the material mesh is written very simply as

$$\psi(\mu, t_n) = \psi(\mu, t_0), \quad \text{for all } t_n \tag{4}$$

where t_0 is the *reference time*, defined as the time when the tags were imposed. The function $\psi(\mu, t_0)$ represents the *initial phase values* on the mesh. Note that the phase values, $\psi(\mu, t_n)$, of a material point are a 3-D vector representing the phase in three linearly independent directions, i.e., $\psi = [\psi_1 \;\; \psi_2 \;\; \psi_3]^T$.

Similar to the 2D-HARP method, phase invariance is used to track motion. However, in the case of 3-D, we have only a limited number of observations of the phase during motion. Specifically, the observations are directly obtained from the HARP images acquired on the SA and LA image planes. The condition, therefore, can be applied only to those points where the mesh intersects with the image planes—the so-called *intersection points*. Mathematically, let $\mu \in M_n$ be a material point on the mesh and also located on an image plane (could be LA or SA) at timeframe n; it will, therefore, have a location, $\boldsymbol{y}$, on the local 2-D coordinate system of the image plane. The phase invariance condition then requires that

$$\psi_k(\mu, t_n) = \phi_k(\boldsymbol{y}, t_n) \begin{cases} k = 1, 2, & \text{for SA images} \\ k = 3, & \text{for LA images} \end{cases} \tag{5}$$

where $\psi_k(\mu, t_n)$ is the phase value of the material point on the mesh and $\phi_k(\boldsymbol{y}, t_n)$ is the observed phase value from the tagged image at timeframe, n. Notice that, on SA tagged images, two components of HARP phase values ($k = 1, 2$) can be observed, whereas on LA tagged images, only one component of HARP phase values ($k = 3$) can be observed. Combining (4) and (5), we get

$$\psi_k(\mu, t_0) = \phi_k(\boldsymbol{y}, t_n) \begin{cases} k = 1, 2, & \text{for SA images} \\ k = 3, & \text{for LA images} \end{cases} \tag{6}$$

which shows that, for the intersection point, the initial phase value of the material point on the mesh should be the same as the observed phase value obtained from the image planes at timeframe, n. The method for tracking of the heart motion is basically to determine the mesh shape at different timeframes so that the phase invariance is always satisfied at the intersection points.

III. Method

A. The Algorithm

A block diagram of 3D-HARP is shown in Fig. 3. First, the material mesh at the reference time—when the tagging sequence is applied—is built. The material properties of the mesh,

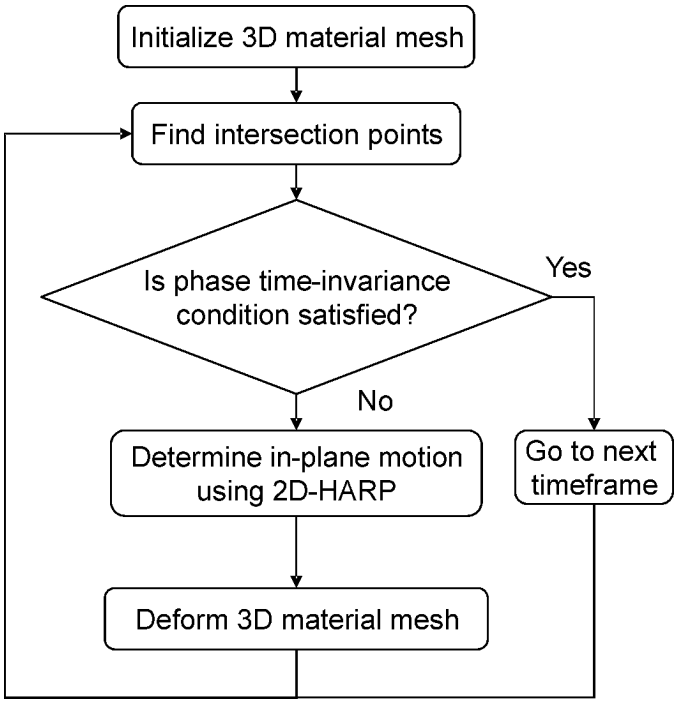

Fig. 3. Block diagram of the algorithm of the material mesh model.

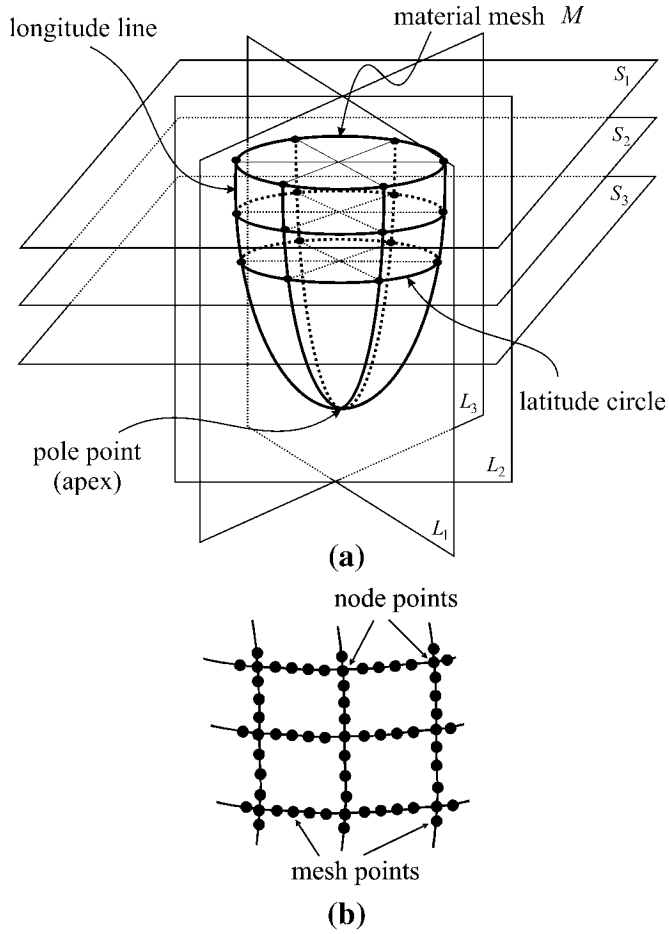

Fig. 4. (a) A material mesh built at the reference time. S_i is an SA image plane and L_j is an LA image plane. M is the material mesh. The material mesh is initialized as latitude circles and longitude lines. (b) The latitude circles and longitude lines are discretized into a collection of mesh points, connected by straight lines. Node points are defined as the junction of latitude circles and longitude lines.

specifically the harmonic phase values, are also initialized at the reference time. Because the tag patterns in the 3-D volume are known at the reference time, the harmonic phase values can be obtained for any material point on the mesh, not just those intersecting the image planes. It is important, however, to state that when tags deform at later timeframes, including even the first timeframe, the HARP values will be unknown except for certain orientations on the image planes. It is expected that the material mesh will not satisfy the phase invariance condition and a discrepancy between $\phi_k(\boldsymbol{y}, t_n)$ and $\psi_k(\mu, t_n)$ will occur.

The phase difference between the initial phase and the observed phase is used (by a 2D-HARP algorithm) to find the apparent motion of all the intersection points where the mesh intersects with the image planes. This apparent motion defines a collection of displacement vectors at the intersection points, and this collection is extended using interpolation to obtain a displacement field on the entire mesh. This displacement field is then used to deform the mesh. After deformation, the phase invariance condition is checked at all intersection points, and if not satisfied, the previous steps are repeated. This deformation process is repeated until the phase invariance condition is satisfied at all the intersection points. After the deformation of the mesh is determined at that timeframe, the algorithm then proceeds to the next timeframe. Having provided this brief overview, we now give the details of each step in the algorithm.

B. Initializing the Material Mesh at the Reference Time

The mesh is constructed to resemble a half elliptical spheroid composing latitude circles and longitude lines [see Fig. 4(a)] where the harmonic phase values are specified. The latitude circles are defined on SA image planes and the longitude lines are defined on LA image planes. The pole point is defined as the junction of longitude lines at the apex. The *node points* are defined as the junction of latitude circles and longitude lines. The longitude lines and latitude circles are discretized into a collection of *mesh points*, connected by straight lines [see Fig. 4(b)]. Therefore, the material mesh is assumed to be a continuous object represented by points with straight line between them. A graphic user interface was built to assist users in this step.

The material mesh should be initialized with respect to the reference time. However, tag application requires several tens of milliseconds before acquisition of the first timeframe. Assuming little heart motion during the tag application, it is feasible to build the mesh using the images at the first timeframe.

After the mesh is built, the initial phase values of all points on it are to be determined. In order to do this, the initial harmonic phase at the reference time is estimated by assuming the tags to be exactly rectilinear when they are applied before any deformation. It is possible then to estimate the initial harmonic phases from tagged images and to extend the estimated phase values into a 3-D volume. We accomplish this by using the tagged images at the first timeframe and estimating the harmonic phases from only static tissues (not moving since the reference time)—since the tags within the myocardium will presumably have already moved. A region of interest (ROI) on

static tissues (usually on liver) is selected on one slice of image. The phase pattern of the tagged image inside this ROI is calculated and extended to 3-D volume. Mathematically, by a simple 1-D example, the phase value of any spatial points x at reference time can be estimated by

$$\phi = W(\omega x + \phi_0) \tag{7}$$

where W is a nonlinear wrapping function, ω and ϕ_0 are tag frequency and phase shift estimated from the tagged image of static tissues, respectively. Therefore, the initial phase values of all the points on the mesh can be estimated.

C. Finding the Intersection Points of the Deformed Mesh on Image Planes

Let us assume that the mesh deformed into a certain shape M_n at timeframe n. We are interested then in finding the shape of the mesh M_{n+1} at the next timeframe $n+1$. First, we assume the initial shape of the mesh at timeframe $n+1$ to be the same as that of timeframe n, i.e., $M_{n+1}^{\langle 0\rangle} = M_n$. This mesh, $M_{n+1}^{\langle 0\rangle}$, then intersects the image planes at timeframe $n+1$. In particular, the longitude lines intersect with SA image planes and the latitude circles intersect with LA image planes (see Fig. 5).

D. Checking the Phase Invariance Condition

As shown in (6), the phase invariance condition must be satisfied at all intersection points. The initial phase value, $\psi(\mu, t_0)$, of the intersection point is obtained from the initial mesh at the reference time. Since the mesh is discretized into a collection of mesh points, it is possible that the intersection point is located between two adjacent mesh points. We use linear interpolation to obtain the initial phase value of the intersection point from the neighboring material points on the mesh. On the other hand, the observed phase value from the image planes can be obtained from the corresponding HARP image. A 2-D phase value $([\phi_1 \ \ \phi_2]^T)$ can be observed for the intersection point of the longitude line and the SA image plane, whereas only a 1-D phase value (ϕ_3) can be observed for the intersection point of the latitude circle and the LA image plane.

The phase invariance condition is then verified at the points of intersection, and the observed phase values of intersection points should agree with their initial phase values. If the condition is not satisfied, the algorithm proceeds to the next step to determine the in-plane motion of intersection points. Otherwise, the algorithm proceeds to the next timeframe.

We must point out the special case that exists at the first timeframe. Since the material mesh is initialized on the image planes, the node points (special case of mesh points) of M_0 are just those intersection points on $M_1^{\langle 0\rangle}$. The initial phases of the mesh points on M_0 are initialized from static tissues (without any deformation), whereas the phases of intersection points on $M_1^{\langle 0\rangle}$ are observed from HARP images inside myocardium (with deformation). The small discrepancy between the two phases enables us to determine the relatively small motion of the myocardium from the reference time to the first timeframe. This motion is small for a normal heart, but in cases like dobutamine stress test, a big motion can be observed—which makes the detection of this motion crucial.

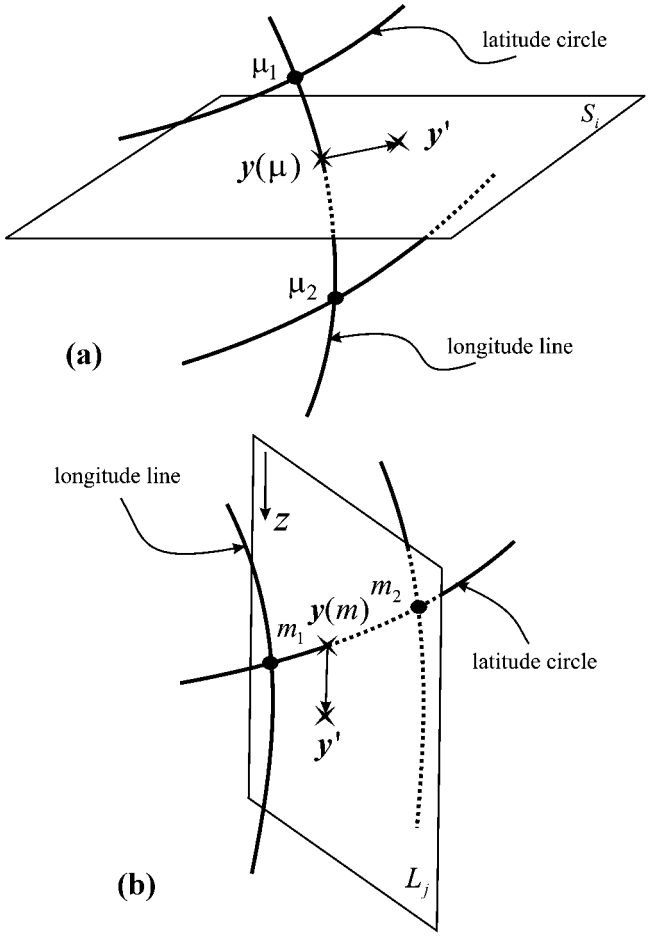

Fig. 5. Diagram of the intersection of the material mesh and image planes, as well as a description of the in-plane motion of intersection points in (a) SA case and (b) LA case. In (a), the material mesh intersects with an SA image plane, S_i. The intersection point $\boldsymbol{y}(\mu)$ is located on both the image plane and the material mesh. $\boldsymbol{y}'$ is the closest point to the intersection point $\boldsymbol{y}(\mu)$ on the image plane S_i that has the same 2-D phase value, $\phi_k(\boldsymbol{y}', \boldsymbol{t}_n)$, as the initial phase value, $\psi_k(\mu, t_0)$, of μ. The displacement vector between $\boldsymbol{y}$ and $\boldsymbol{y}'$ describes the in-plane 2-D motion of the intersection point, $\boldsymbol{y}(\mu)$. Similarly, in (b), the material mesh intersects with an LA image plane, L_j, at the intersection point $\boldsymbol{y}(\mu)$, and $\boldsymbol{y}'$ is the closest point to the intersection point $\boldsymbol{y}(\mu)$ on the image plane L_j that has the same 1-D phase value, $\phi_k(\boldsymbol{y}', \boldsymbol{t}_n)$, as the initial phase value, $\psi_k(\mu, t_0)$, of μ. The displacement vector between $\boldsymbol{y}$ and $\boldsymbol{y}'$ describes the in-plane 1D motion of the intersection point, $\boldsymbol{y}(\mu)$.

E. Determining In-Plane Motion of Intersection Points Using 2D-HARP

In the case where the phase invariance condition is not satisfied, the difference between the two phase values, ψ and ϕ, is used to find the in-plane apparent motion of the intersection points using 2D-HARP. For the intersection point on SA planes, we use the 2D-HARP tracking method to search around the intersection point on the image plane to find the closest point, $\boldsymbol{y}'$, that has the same 2-D phase value as the initial phase value of the intersection point, which means

$$\psi_k(\mu, t_0) = \phi_k(\boldsymbol{y}', t_n) \quad k = 1, 2 \tag{8}$$

are satisfied.

For the intersection point on LA planes, only a 1-D phase value is available, and one more step is needed to use 2D-HARP tracking. We create a synthetic HARP image that simulates straight vertical tag lines applied on LA images. In this sense, the 2D-HARP tracking is restricted to 1-D so that the new

point, $\boldsymbol{y}'$, is either above or below the intersection point on the LA image. This means that

$$\psi_k(\mu, t_0) = \phi_k(\boldsymbol{y}', t_n) \quad k = 3 \tag{9}$$

is satisfied, where in this case, $\boldsymbol{y}'$ is the closest point to the intersection point on the LA image plane.

The displacement between the new point and the intersection point describes the in-plane apparent motion of the intersection point. It generates a displacement vector on the image plane at the intersection point. The discrete displacement vectors generated on all the intersection points form a displacement field that deforms the mesh. It should be noted that the displacement vectors generated on the longitude lines are on SA planes, and these vectors relate to the concentric contraction of the ventricle and its twisting, while those generated on the latitude circles are on the LA planes, and they relate to the longitude compression of the ventricle—the motion of the base toward the apex. Fig. 5 shows what we have described in the above section.

F. Deforming the Mesh Using the Displacement

The displacement field generated on all the intersection points is interpolated to obtain the displacements on all the mesh points. Each displacement vector obtained by 2D-HARP behaves like an impulse applied at the intersection point. Therefore, the interpolation is implemented by applying a kernel at intersection points to diffuse the estimated displacements derived from 2D-HARP to other points on the mesh. The diffused displacements from all the intersection points are superimposed simultaneously to obtain the final 3-D displacements at all the mesh points. The kernel used to diffuse the displacements is designed as a Gaussian-function that influences the neighboring points based on the distance on the mesh. The size of the kernel affects the area through which the impulse spreads. Therefore, the displacements on all the mesh points acquired by interpolation deform the mesh to a new shape $M_{n+1}^{\langle 1 \rangle}$.

G. Iterating Until the Phase-Time Invariance Condition is Satisfied

The resulting deformed mesh, $M_{n+1}^{\langle 1 \rangle}$, intersects with image planes and the new intersection points are obtained. The phase invariance condition is checked again at the points of intersection to determine whether this condition is satisfied after deformation. If the condition is not satisfied, the steps are repeated and a sequence of meshes ($M_{n+1}^{\langle 2 \rangle}$, $M_{n+1}^{\langle 3 \rangle}, \ldots$) is generated until the phase invariance condition is adequately satisfied.

Mathematically, to define the convergence condition of this iterative algorithm, we define $\boldsymbol{\psi}_k$ and $\boldsymbol{\phi}_k$ as the initial phase vectors and the observed phase vectors of all intersections points, respectively, and also define the difference between these two vectors as

$$\varepsilon_k = |W(\boldsymbol{\psi}_k - \boldsymbol{\phi}_k)| \quad k = 1, 2, 3. \tag{10}$$

The convergence condition is defined as

$$\max(\log_{10} \varepsilon_k) < -3 \quad k = 1, 2, 3. \tag{11}$$

When the convergence condition, or the phase invariance condition, is satisfied, the iterations are then terminated and the most recent deformation is considered as the new shape of the mesh at that timeframe. The algorithm then proceeds to the next timeframe and the steps are repeated.

IV. Experiments and Results

A. Experiment

To demonstrate the ability of this method to track the 3-D motion of the heart, we performed experiments on a normal volunteer. The image dataset consists of two SA sets (6 parallel slices with horizontal and vertical tag lines) and one LA set (6 radial slices, 30° apart, with horizontal tag lines) of tagged images. The images were acquired on a GE 1.5T Signa scanner (GE Medical Systems, Milwaukee) after the subject gave written informed consent. A SPAMM (SPAcial Modulation of Magnetization) sequence was used to generate stripe tags. The imaging parameters were: $\mathrm{FOV} = 360\ \mathrm{mm}$, $\mathrm{slice\ thickness} = 7\ \mathrm{mm}$, $\mathrm{matrix\ size} = 256 \times 128$, $\mathrm{tag\ spacing} = 5.5\ \mathrm{mm}$, $\mathrm{flip\ angle} = 12$. The in-plane spatial resolution is 1.4 mm × 2.8 mm. All the images were acquired at the end of exhalation. The cine image sequence for each tagging direction on each slice was acquired in one breath-hold and the complete dataset was acquired in 18 breath-holds. A total of nine timeframes, covering systole, were acquired with a time interval of 33 ms.

The 3D-HARP algorithm was implemented on a 1.1-GHz Intel Pentium III processor (with 512 Mbytes RAM) using MATLAB (Mathworks, Inc.) in a software program with a graphic user interface. Following the steps of the algorithm described previously, the initial 3-D mesh was manually created at only the first timeframe (end-diastole) inside the myocardium—this is the only step that requires human interaction. The subsequent steps of mesh point tracking were totally automatic. The mesh was initialized as 6 latitude circles and 12 longitude lines. The apex was specified on the LA images. Between each node point (junction of latitude circles and longitude lines), four other mesh points were initialized by interpolation. A total of 649 mesh points were generated. On the SA image planes, the left ventricle was divided into 12 segments (ordered clockwise, viewed from the apex) by the intersection with the longitude lines, with five mesh points on each segment. The starting point of the first segment was set on the midseptum. The deformation of the mesh at each timeframe converged to satisfy the phase invariance condition in less than 10 iterations per timeframe. The total time for building and tracking the mesh was about 8 min.

Fig. 6(a) shows the deformation of the material mesh at different stages during systole, beginning with the initial mesh at the reference time, built manually at end-diastole. As can be seen, the tracked mesh shows the typical mechanics of the normal left ventricle during systole: the compression of the heart along the long-axis caused by the motion of the base toward the apex, and the gradual change in twist pattern due to the different rotation angles between the slices.

The observed deformation of the mesh was quantified from the coordinates of the mesh points during systole. By measuring the percentile change in segment length on the latitude circles, we were able to measure the $\mathrm{E_{CC}}$. Fig. 7 shows the $\mathrm{E_{CC}}$ strain plots of the 12 segments on the left ventricle. Each plot shows the $\mathrm{E_{CC}}$ strain by slices. As can be seen, the lateral systolic $\mathrm{E_{CC}}$ strain (segs 6 and 7), ranging from 20 to 30 percent, is greater than that of the septal strain (segs 1 and 12), which is around 10 to 20 percent. Another observation is that at the lateral side (segs 7 and 8), the apical slices seem to have greater strain than

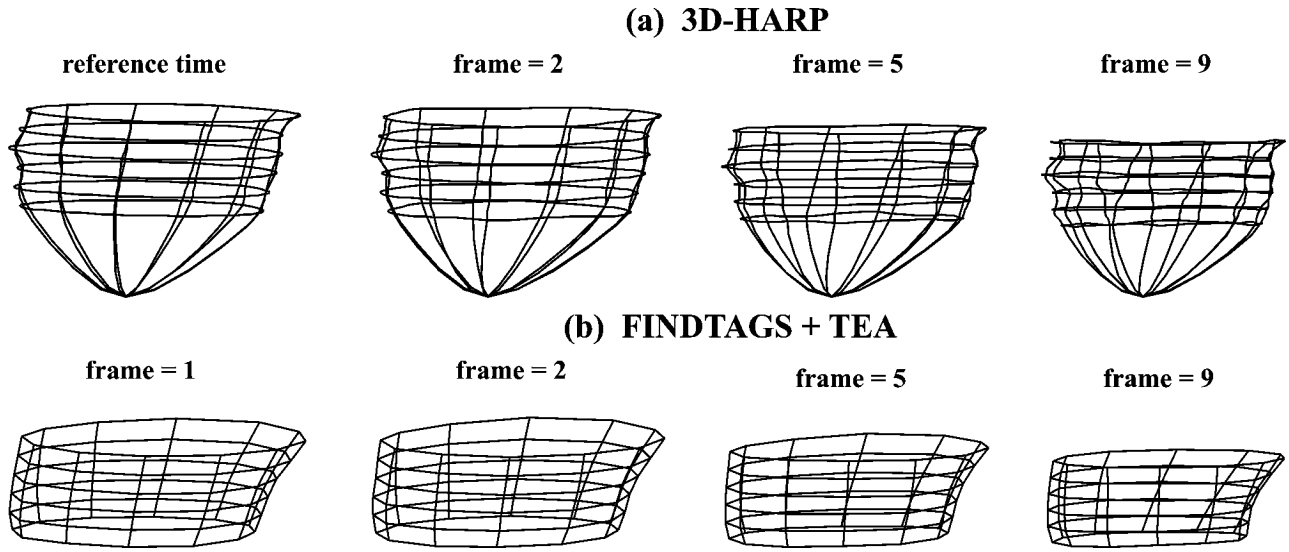

Fig. 6. Mesh deformation at 4 timeframes. (a) Mesh deformation estimated by 3D-HARP. The reference time, at end diastole, is the time when the tags are imposed and timeframe 9 is at end systole. (b) Mesh deformation estimated by FINDTAGS+TEA.

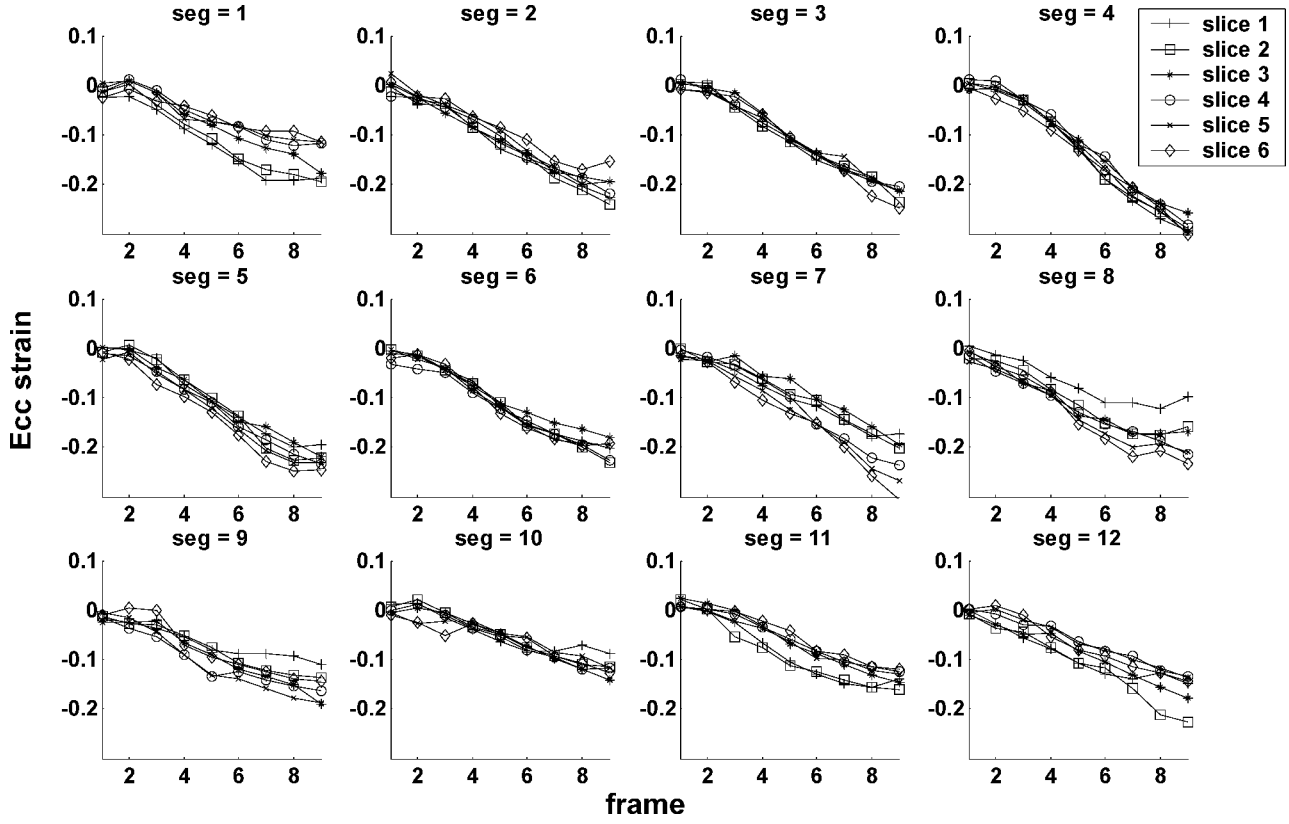

Fig. 7. Ecc strain plots of the 12 segments on the left ventricle. Each plot shows the Ecc strain by slice. The segmentation starts from the midseptum, and goes around the left ventricle clockwise (viewed from the apex). Segs 1 and 12 can be considered septal segments and segs 6 and 7 can be considered lateral segments. The order of SA slices is from base to apex (slice 1 to slice 6). All six slices were acquired at the midventricular position.

the basal slices. However, at the septal side (segs 1 and 2), this relationship is reversed, i.e., the more basal slices have greater strain than that of more apical slices. Fig. 8 shows the corresponding 3-D E_{CC} strain map on 9 timeframes of deformed material mesh. The color of each patch represents the averaged strain of one segment at one SA slice level.

The twist angle of a specific slice is defined as the net rotation angle of that slice from end-diastole to the current timeframe. A counterclockwise rotation (viewed from apex) is defined as positive. Fig. 9 shows the twist angle plots of the 12 segments around the long axis. Each plot shows the twist angle by slice. A gradual change of the twist pattern by slice and segment can be clearly examined on the plot. To better observe the trend of twist by slices, we took the average of the twist angles over 12 segments on each slice. From Fig. 10(a), we can observe that, at early systole, all slices rotate counterclockwise (viewed from the apex). Later in systole, basal slices reverse their rotation direction and plateau at late systole, whereas more apical slices

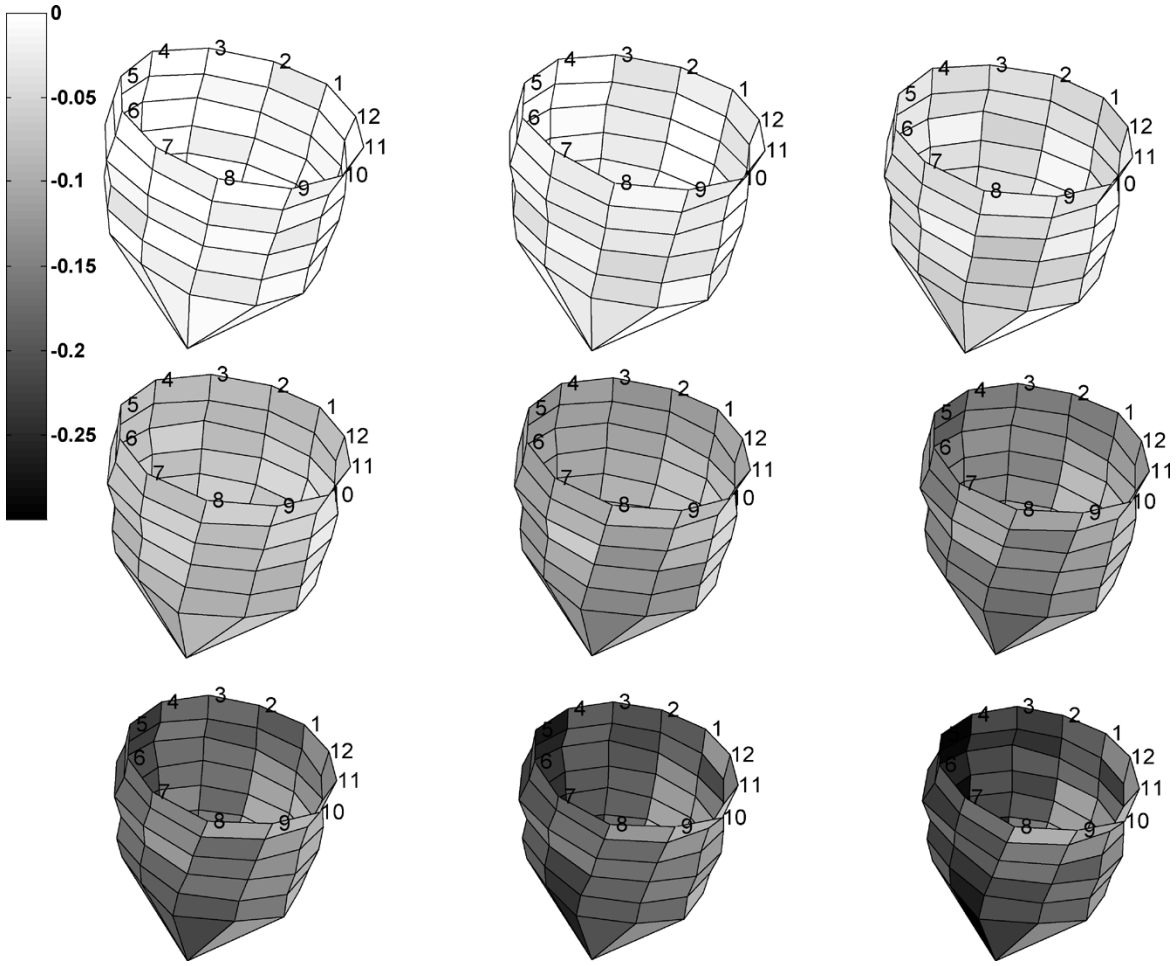

Fig. 8. The 3-D Ecc strain map in 9 timeframes of deformed material mesh. The color of each patch represents the averaged Ecc strain of one segment at one SA slice level. 1 to 12 are the segment indices.

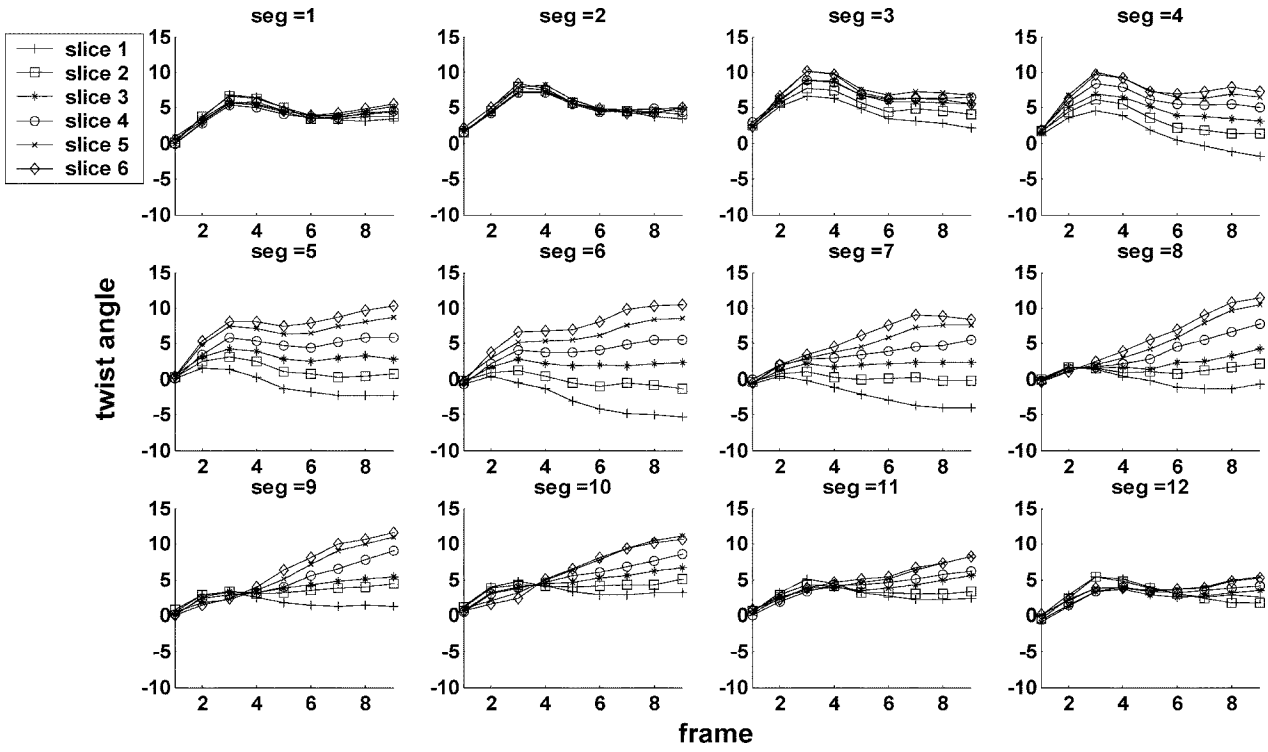

Fig. 9. Twist angle plots of the 12 segments on the left ventricle. Each plot shows the twist angle by slices, ordered from base to apex (slice 1 to slice 6).

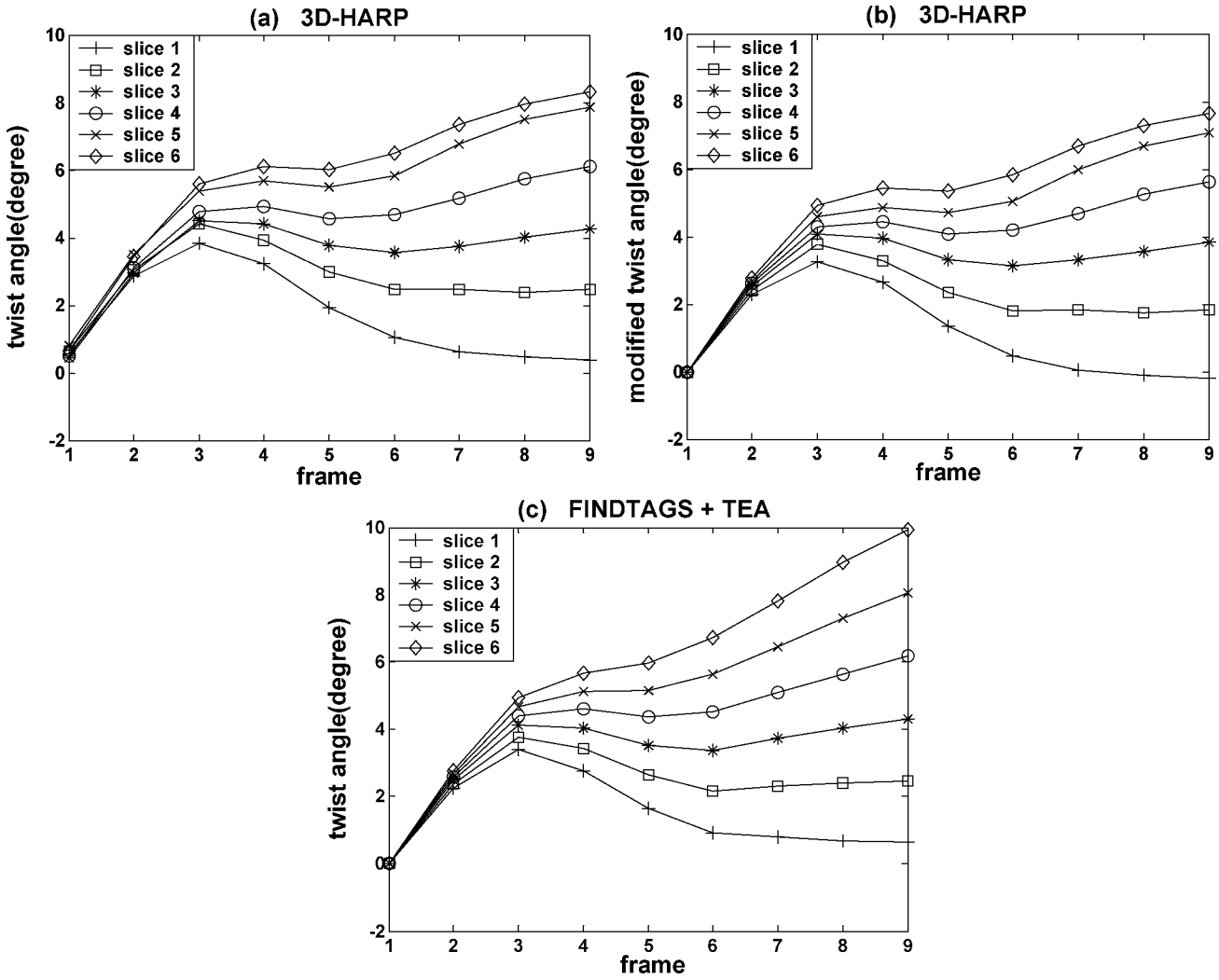

Fig. 10. (a) Average twist angles over 12 segments on the six slices, obtained by 3D-HARP. The reference time is the time of applying tags. (b) To compare with FINDTAGS+TEA, a modified average twist angle plot is generated by 3D-HARP. The reference time is the first timeframe. (c) Average twist angle over 12 segments on the six slices, obtained by FINDTAGS+TEA. The reference time is the first timeframe.

maintain the trend of rotation throughout systole. This result is consistent with what was reported by Lorenz *et al.* [22].

Note that both the twist angles and the $\mathrm{E_{CC}}$ strain do not begin at zero at the first timeframe. This is because in 3D-HARP, we use the time point when tags are applied as the reference time, rather than the first timeframe. Thus, from the reference time to the first timeframe (a 53.5-ms delay in this dataset), both a small twist and a small strain are observed.

B. Validation

Since FINDTAGS [5], [6] and TEA [11] are considered to be a gold standard in the estimation of 3-D cardiac motion and strain, we used these two programs to validate our results. FINDTAGS was used to perform the segmentation of endo- and epicardium, as well as the identification of tag lines. TEA was used to generate the mesh and the circumferential strain values. For comparison, a mesh composed of 12 segments and 6 slices was generated by TEA. The starting point of the first segment was also set at the midseptum, which ensured that the mesh generated by TEA had a similar initial mesh position as that of 3D-HARP. The series of deformed mesh in TEA was obtained by displacement field fitting of the tracked tag lines. The processing in FINDTAGS and TEA required approximately 4 h and 1/2 h, respectively. Fig. 6(b) shows the 3-D deformed mesh output by TEA. Visually, the motion pattern is similar to the output of 3D-HARP, as shown in Fig. 5(a). Notice the similar compression toward the apex and twist of different slices.

To quantify the comparison, we took the average of the twist angles over 12 segments on each slice using 3D-HARP and FINDTAGS+TEA, respectively. One thing we had to consider was that, since 3D-HARP uses the time point of applying tags as the reference time, which is different from FINDTAGS+TEA, in which the first timeframe is used, we had to modify the output of 3D-HARP by eliminating this factor of difference for comparison. The resulting measurements are called *modified twist angle*. Thus, both methods now have twist angles starting from zero, as shown in Fig. 10(b) and (c). Notice both methods have very similar twist patterns on the same slices.

A statistical comparison was also performed for $\mathrm{E_{CC}}$ strain values and twist angles. The regression coefficients between 3D-HARP and FINDTAGS+TEA were $r^2 = 0.8605$ for $\mathrm{E_{CC}}$ strain, with the regression equation $y = 1.0247x - 0.0064$ [see

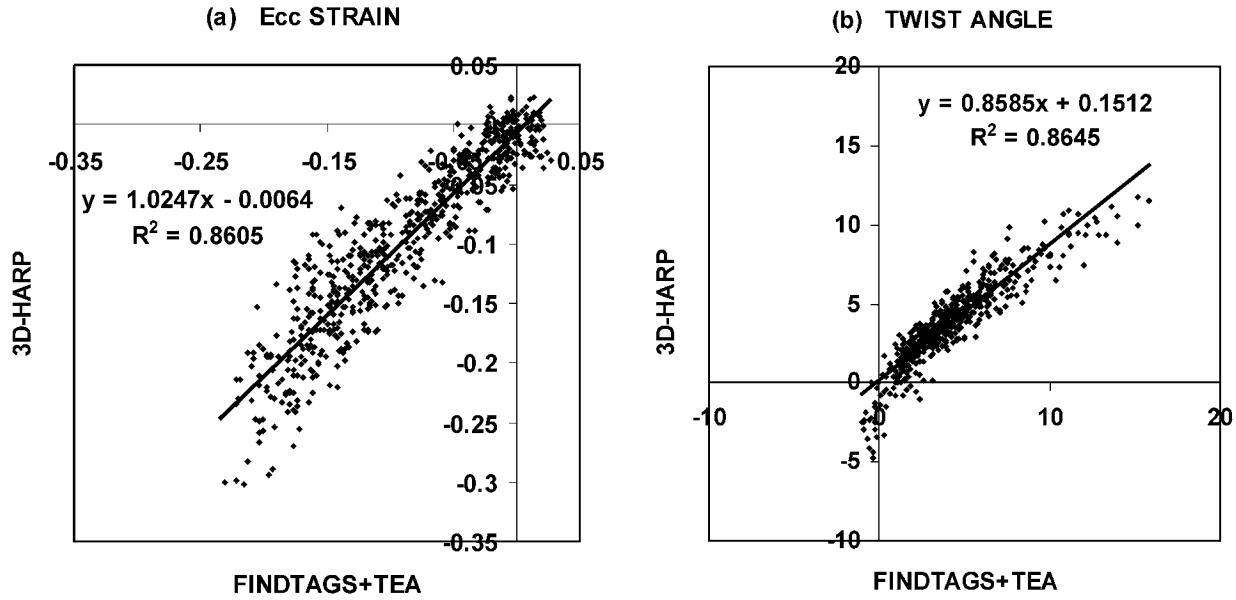

Fig. 11. Correlation between cardiac motion measures as assessed by 3D-HARP(y axis) and FINDTAGS+TEA(x axis) for Ecc (a) and twist angle (b).

Fig. 11(a)]. For twist angles, the regression coefficients between the two methods were $r^2 = 0.8645$, with the regression equation as $y = 0.8585x + 0.1512$ [see Fig. 11(b)].

One fact should be stressed here: since 3D-HARP and FINDTAGS+TEA are two different techniques, the initial meshes are generated differently. As for 3D-HARP, the mesh is initialized on the image planes, whereas FINDTAGS+TEA generates the initial mesh by tag surface fitting. Therefore, the initial mesh points generated by the two methods are located at the same regions but not the exact same positions. We would expect better correlation between these two methods if the two initial meshes were exactly the same.

V. Discussion

In the proposed technique, the phase invariance condition was used both to drive the deformation of the mesh and to guarantee a proper termination. Since at each timeframe, the phase value is checked to match the initial phase values at the reference time, it limits the accumulation of error during tracking from one timeframe to the other.

Several issues must be addressed and will be the subject of future research. First, further investigation of the appropriate mechanical model for the material mesh is needed. In this paper, we used interpolation to deform all the points of the mesh from the displacement vectors at the points of intersection. However, we would like to consider the displacement vectors as a discrete force that deforms the mesh. In this case, we need to assume that the mesh possesses certain mechanical properties same as that of the heart tissue. A more realistic model can be derived so that more accurate and faster convergence could be achieved. Second, although the algorithm converged correctly in experiments we have performed to date, further investigation is required to determine the necessary and sufficient conditions to guarantee convergence. Third, a single-layer mesh inside the LV wall was created in this example. This method could be easily extended to build a multi-layer mesh that would enable the computation of transmural strain values and create a 3-D strain tensor map. Careful considerations are required since meshes close to the epicardium and the endocardium will be more prone to noise. Finally, the algorithm is currently implemented in Matlab (Mathworks Inc.), but we expect it to be much faster if implemented in C or C++.

VI. Conclusion

Three-dimensional–HARP (3D-HARP) is a fast, semiautomatic analysis technique to track 3-D cardiac motion and perform regional motion analysis. There are a number of advantages to the proposed technique. First, required computations are fast since segmentation is not necessary to track motion. Initialization of the material mesh is the only step that requires human interaction. Second, deformation is always checked based on the phase invariance condition, which guarantees the proper deformation. This condition-checking step eliminates the accumulation of error from one timeframe to the next. Third, the small amount of motion between the time of applying tags and the first timeframe can be estimated, which is not possible with FINDTAGS+TEA. Finally, the technique does not require a rigid form of the mesh, and a smaller, partial mesh that covers only small regions in the LV could be used. This would allow faster motion tracking of this region.

Acknowledgment

The authors would like to thank Dr. W. S. Kerwin from the University of Washington for his kind help with data acquisition. They also would like to acknowledge the help of M. Guttman and Dr. E. McVeigh and Dr. W. O'Dell for kindly providing the FINDTAGS and TEA software.

References

[1] L. C. Palmon, N. Reichek, S. B. Yeon, N. R. Clark, D. Brownson, E. Hoffman, and L. Axel, "Intramural myocardial shortening in hypertensive left ventricular hypertrophy with normal pump function," *Circulation*, vol. 89, no. 1, pp. 122–131, 1994.

[2] E. A. Zerhouni, D. M. Parish, W. J. Rogers, A. Yang, and E. P. Shapiro, "Human heart: tagging with MR imaging—a method for noninvasive assessment of myocardial motion," *Radiology*, vol. 169, no. 1, pp. 59–63, 1988.
[3] L. Axel and L. Dougherty, "MR imaging of motion with spatial modulation of magnetization," *Radiology*, vol. 171, pp. 841–845, 1989.
[4] L. Axel, "Biomechanical dynamics of the heart with MRI," *Annu. Rev. Biomed. Eng.*, vol. 4, pp. 321–347, 2002.
[5] M. A. Guttman, J. L. Prince, and E. R. McVeigh, "Tag and contour detection in tagged MR images of the left ventricle," *IEEE Trans. Med. Imag.*, vol. 13, no. 1, pp. 74–88, Mar. 1994.
[6] M. A. Guttman, E. A. Zerhouni, and E. R. McVeigh, "Analysis of cardiac function from MR images," *IEEE Comput. Graph. Appl.*, vol. 17, no. 1, pp. 30–38, Jan.-Feb. 1997.
[7] T. S. Denney, "Estimation and detection of myocardial tags in MR image without user-defined myocardial contours," *IEEE Trans. Med. Imag.*, vol. 18, no. Apr., pp. 330–344, 1999.
[8] T. S. Denney, "Unsupervised reconstruction of a three-dimensional left ventricular strain from parallel tagged cardiac images," *Magn. Reson. Med.*, vol. 49, pp. 743–754, 2003.
[9] A. F. Frangi, W. J. Niessen, and M. A. Viergever, "Three-dimensional modeling for functional analysis of cardiac images: a review," *IEEE Trans. Med. Imag.*, vol. 20, no. 1, pp. 2–25, Jan. 2001.
[10] J. Declerck, T. S. Denney, C. Ozturk, W. O'Dell, and E. R. McVeigh, "Left ventricular motion reconstruction from planar tagged MR images: a comparison," *Phys. Med. Biol.*, vol. 45, pp. 1611–1632, 2000.
[11] W. G. O'Dell, C. C. Moore, W. C. Hunter, E. A. Zerhouni, and E. R. McVeigh, "Three-dimensional myocardial deformations: calculation with displacement field fitting to tagged MR images," *Radiology*, vol. 195, no. 3, pp. 829–835, 1995.
[12] J. Huang, D. Abendschein, V. G. Davila-Roman, and A. A. Amini, "Spatio-temporal tracking of myocardial deformations with a 4-D B-spline model from tagged MRI," *IEEE Trans. Med. Imag.*, vol. 18, no. 10, pp. 957–972, Oct. 1999.
[13] Y. P. Wang, Y. Chen, and A. A. Amini, "Fast LV motion estimation using subspace approximation techniques," *IEEE Trans. Med. Imag.*, vol. 20, no. 6, pp. 499–513, Jun. 2001.
[14] X. Deng and T. S. Denney, "Three-dimensional myocardial strain reconstruction from tagged MRI using a cylindrical B-spline model," *IEEE Trans. Med. Imag.*, vol. 23, no. 7, pp. 861–867, Jul. 2004.
[15] A. A. Young, "Model tags: direct three-dimensional tracking of heart wall motion from tagged magnetic resonance images," *Med. Imag. Anal.*, vol. 3, no. 4, pp. 361–372, 1999.
[16] W. S. Kerwin and J. L. Prince, "Cardiac material markers from tagged MR images," *Med. Imag. Anal.*, vol. 2, no. 4, pp. 339–353, 1998.
[17] N. F. Osman, W. S. Kerwin, E. R. McVeigh, and J. L. Prince, "Cardiac motion tracking using CINE harmonic phase (HARP) magnetic resonance imaging," *Mag. Reson. Med.*, vol. 42, pp. 1048–1060, 1999.
[18] N. F. Osman, E. R. McVeigh, and J. L. Prince, "Imaging heart motion using harmonic phase MRI," *IEEE Trans. Med. Imag.*, vol. 19, no. 3, pp. 186–202, Mar. 2000.
[19] S. Ryf, M. A. Spiegel, M. Gerber, and P. Boesiger, "Myocardial tagging with 3D-SPAMM," *J. Magn. Res. Imag.*, vol. 16, pp. 320–325, 2002.
[20] I. Haber and C. F. Westin, "Model-based 3D tracking of cardiac motion in HARP images," presented at the *Int. Soc. Mag. Reson. Med.*, Honolulu, HI, May 10, 2002.
[21] N. F. Osman and J. L. Prince, "Visualizing myocardial function using HARP MRI," *Phys. Med. Biol.*, vol. 45, pp. 1665–1682, 2000.
[22] C. H. Lorenz, J. S. Pastorek, and J. M. Bundy, "Delineation of normal human left ventricular twist throughout systole by tagged cine magnetic resonance imaging," *J. Cardiovasc. Magn. Reson.*, vol. 2, no. 2, pp. 97–108, 2000.

Li Pan received the B.E. and M.E. degrees in biomedical engineering from the Department of Electrical Engineering, Tsinghua University, Beijing, China, in 1996 and 1999, respectively. Since 1999, she has been working towards the Ph.D. degree in the Department of Biomedical Engineering, Johns Hopkins School of Medicine, Baltimore, MD.

Her research interests include cardiac magnetic resonance imaging (MRI), medical image analysis, and signal and image processing. Her special interests are MR-tagged image analysis, three-dimensional cardiac motion tracking, noninvasive quantification of regional myocardial function, and coronary artery imaging.

Jerry L. Prince (S'78–M'83–SM'96–F'04) received the B.S. degree from the University of Connecticut, Storrs, in 1979 and the S.M., E.E., and Ph.D. degrees in 1982, 1986, and 1988, respectively, from the Massachusetts Institute of Technology, Cambridge, all in electrical engineering and computer science.

After receiving the Ph.D. degree on the subject of geometric reconstruction in computed tomography, he joined the technical staff at The Analytic Sciences Corporation (TASC), Reading, MA, where he contributed to the design of an automated vision system for synthetic aperture radar imaging. He joined the faculty of Johns Hopkins University, Baltimore, MD, in 1989, where he has been a Professor with the Department of Electrical and Computer Engineering since 1998. He has held the William B. Kouwenhoven Chair since 2001. He holds joint appointments in the Departments of Radiology, Biomedical Engineering, Applied Mathematics and Statistics, and Computer Science. From 2001 to 2004, he was the Associate Director for Research in the Engineering Research Center for Computer Integrated Surgical Systems and Technology. Over the past 15 years, he has published numerous book chapters and peer-reviewed journal and conference papers. He coedited the book *Measurement of Cardiac Deformations from MRI: Physical and Mathematical Models* (with A.A. Amini) (Dordrecht: Kluwer Academic, 2001). His current research interests are in image processing and computer vision with application to medical imaging. His major projects include magnetic resonance imaging of cardiac motion, three-dimensional brain image analysis, and X-ray computed tomography.

Dr. Prince has served as an Associate Editor for both the IEEE TRANSACTIONS ON IMAGE PROCESSING and the IEEE TRANSACTIONS ON MEDICAL IMAGING. He is on the Editorial Board of *Medical Image Analysis* and is a member of Sigma Xi professional society and Tau Beta Pi, Eta Kappa Nu, and Phi Kappa Phi honor societies. He was a member of the IEEE Signal Processing Society Image and Multidimensional Signal Processing (IMDSP) Technical Committee from 1994 to 2000. He has received several awards, including the 1993 National Science Foundation Presidential Faculty Fellows Award and the 1997 Maryland Outstanding Young Engineer Award.

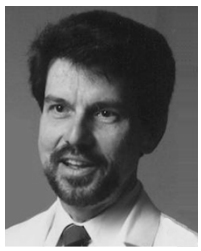

João A. C. Lima received the M.D. degree from the School of Medicine of the Federal University of Bahia, Salvador, Brazil, in 1977 and the M.B.A. degree from Johns Hopkins University, Baltimore, MD, in 2001.

He completed his cardiology fellowship in 1990 at Johns Hopkins University and, upon completion, joined the faculty of the University of Pennsylvania, Philadelphia. In 1992, he returned to Johns Hopkins University, where he is currently an Associate Professor with the Department of Medicine. He also holds a joint appointment with the Department of Radiology and Epidemiology. He is the Director of Cardiovascular Imaging in Cardiology. His research interests are concentrated on the development and application of imaging and technology to address scientific and clinical problems involving the heart and vascular system. His efforts have been directed to the development of magnetic resonance (MR) contrast techniques to investigate microvascular function in patients and experimental animals with myocardial infarction; functional reserve secondary to dobutamine stimulation and myocardial viability assessed by sodium imaging; cardiac MR and computed tomography program development of techniques to characterize atherosclerosis in humans with cardiovascular or cerebrovascular disease.

Nael F. Osman (S'95–M'00) received the B.Sc. and M.S degrees from the Department of Electronics and Communications, Faculty of Engineering, Cairo University, Cairo, Egypt, in 1992 and 1995, respectively. He received the Ph.D. degree in electrical and computer engineering from Johns Hopkins University, Baltimore, MD, in 2000.

Currently, he is an Assistant Professor with the Department of Radiology and Radiological Science, Johns Hopkins University. He also holds a joint appointment with the Department of Electrical and Computer Engineering. His research interests include signal and image processing, medical imaging, and magnetic resonance imaging (MRI). Special interests are in noninvasive imaging of mechanical properties of tissue and quantitative assessment of regional function of the heart.